Restratification after Deep Convection

HELEN JONES AND JOHN MARSHALL

Department of Earth, Atmospheric and Planetary Sciences, Massachusetts Institute of Technology, Cambridge, Massachusetts

(Manuscript received 5 August 1996, in final form 23 April 1997)

ABSTRACT

An important, yet poorly understood, aspect of the water mass transformation process in the ocean is the manner in which the convected fluid, once formed, is accommodated and drawn into the general circulation. Following ''violent mixing'' in the open ocean that creates a deep homogenous body of fluid, restratification of the surface (~500 m) layer is observed to occur rapidly, sealing over the convection patch. Recent hydrographic casts and tomography inversions in the Gulf of Lions by Send et al., for example, show that very quickly, within a week or so of the cessation of cooling, a stratified near-surface layer develops on top of the mixed patch. This restratification occurs much more rapidly than can be accounted for by air–sea fluxes.

By analytical and numerical study the authors argue that advection by geostrophic eddies spawned by the baroclinic instability of the mixed patch is likely to be a principal mechanism by which restratification occurs. A restratification timescale, $\tau_{\text{restrat}} \approx 5\delta r/(Nh)$, where r is the radius of the patch of mixed water, h its depth, and N the ambient stratification, can be deduced from the magnitude of the lateral buoyancy flux associated with the geostrophic eddy field. This formula finds support from numerical results and is in broad agreement with the observations. Finally the results of the study are used to interpret recent field observations in the Labrador and Mediterranean Seas.

1. Introduction

a. Background

The process of water mass transformation in deep oceanic convection can be usefully divided into three phases: preconditioning, violent mixing, and spreading (MEDOC Group 1970). Preconditioning involves the conditioning of a particular site, rendering it susceptible to convection. Violent mixing creates and maintains, through highly energetic plume-scale overturning (Jones and Marshall 1993), a large dense body of fluid that is extremely homogeneous in its tracer properties (the mixed patch is commonly, but somewhat misleadingly, referred to as a ''chimney''). The simultaneous slumping and geostrophic adjustment of the heavy mixed patch results in the development of a peripheral rim current in ''thermal wind'' balance, cyclonic above and anticyclonic below. This current is susceptible to baroclinic instability spawning Rossby-radius-scale eddies that play a central role in the subsequent evolution and spreading of the convectively processed waters.

The spreading phase, which is the subject of this paper, typically follows the cessation of intense surface buoyancy forcing. We elucidate and quantify one of the primary mechanisms—baroclinic instability—which controls the rate at which fluid, mixed by convection, spreads away from its formation region and stratified peripheral fluid is drawn in to the convection region, returning the site to its preconvection state.

b. Observations

Observations of the integral effects of convection on the environment of the convection site are rather scarce. In particular there is only fragmentary evidence of the development of geostrophic eddies and of their net flux exchange with the environmental water masses and associated timescales. An effective way to monitor the three-dimensional development of water masses transformed by convection, however, is through acoustic tomography from sound sources that are distributed within and around the regime. Experiments of this kind were recently carried out in the Greenland Sea (Worcester et al. 1993) and in the Gulf of Lions (THETIS Group 1994; Send et al. 1995). Tomography made it possible to monitor the presence of the Levantine Intermediate Water (LIW) temperature maximum at a depth of 150–500 m during and in the aftermath of convection in the Gulf of Lions. For example, Fig. 1 (taken from Send et al. 1995, Fig. 9) plots the fraction of stratified water present, integrated over the convection site and in the LIW layer, as a function of time; the thin straight lines give

Corresponding author address: Dr. John Marshall, Dept. of Earth, Atmospheric and Planetary Sciences, MIT, Room 54-1526, Cambridge, MA 02139.
E-mail: marshall@gulf.mit.edu

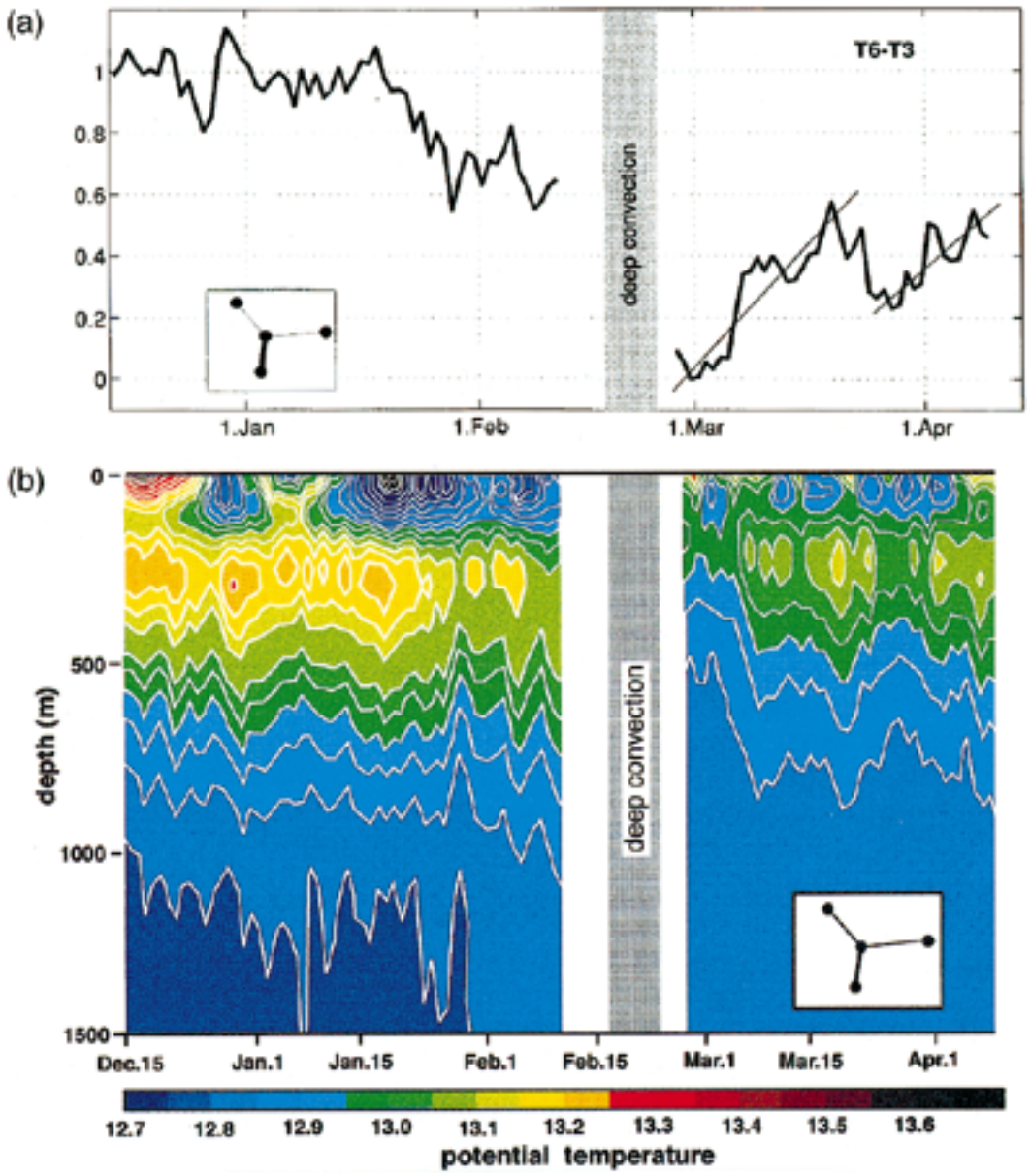

FIG. 1. (a) The fraction of stratified water present, integrated over the convection site in the Gulf of Lion in the 150 → 500-m layer, as a function of time during winter 1994. The thin straight lines give estimates of the warming rate during restratification and suggest a timescale for restratification for a mixed patch, 50 km in diameter and 1600 m deep, of ~40 days. The inset shows a triangle of side 100 km. (b) Time evolution of the range-averaged potential temperature over a convection patch as a function of depth. Following deep convection there is a rapid near-surface restratification to a depth of a few hundred meters (taken from Send et al. 1995, Fig. 9).

estimates of the ''warming rate'' during restratification. The color plate shows the time evolution of the range-averaged potential temperature over the convection patch as a function of depth. They concluded that the deep-mixed patch was reoccupied by LIW on a timescale of about 40 days. Of course, such an integral measure does not allow one to identify mechanisms or distinguish between mean and eddy exchange.

Although it is not feasible to directly monitor eddy correlations over a sufficiently wide area to make them useful, field observations clearly show that vigorous geostrophic eddy activity occurs concomitantly with, and after, violent convective mixing.

c. *Approach*

Our approach in this work is to identify and characterize a likely restratification mechanism—transport

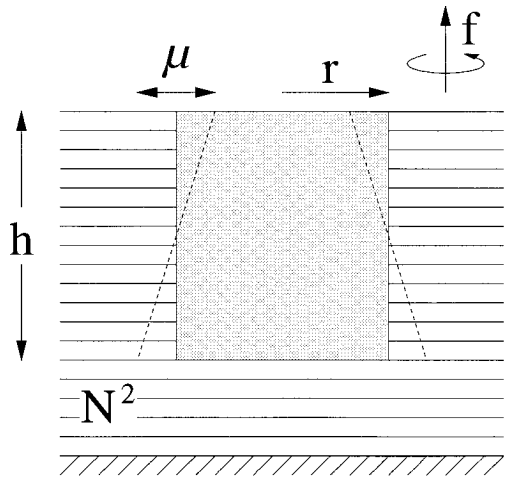

FIG. 2. Schematic diagram of a mixed patch. We suppose that, in the aftermath of convection, a large mixed cylinder of fluid of radius r and depth h remains. Outside the cylinder the ocean takes on its ambient stratification N, assumed constant. In the region where the mixed patch joins the ambient fluid, of width μ, strong lateral density gradients will exist that, in the presence of rotation, support a thermal wind, creating a rim current around the mixed column.

by geostrophic eddies—that might explain the above observations. We begin by abstracting from the natural (and inherently complicated) system a highly simplified one governed by only a few external parameters. We suppose that, in the aftermath of convection, there remains a large mixed cylinder of fluid, of radius r and depth h, as sketched schematically in Fig. 2. Outside the cylinder the ocean takes on its ambient stratification N, assumed constant. In the region where the mixed patch abuts the ambient fluid, of width μ, strong lateral density gradients will exist that, in the presence of rotation, support a thermal wind creating a ''rim current'' around the mixed column.

If the radius of the mixed patch is greater than the Rossby radius of deformation $L_\rho = Nh/f$, then it is prone to baroclinic instability. Indeed, in Fig. 3 we present results from a numerical calculation in which a cylinder of dense homogeneous fluid was placed in an initially resting stratified fluid and allowed to evolve in the absence of external forcing. The radius of the cylinder is 50 km, greatly exceeding the deformation radius L_ρ, here 4 km. Initially the edges of the column merely slump as the dense fluid sinks and spreads under the influence of gravity. But the spreading is limited (initially) to a deformation radius by rotation as azimuthal (rim) currents—cyclonic on top, anticyclonic below—are set up in thermal wind balance with the lateral density gradients at the edge of the column. Subsequently, however, baroclinic eddies grow (here a mode-14 instability consistent with linear theory reviewed in the appendix), reach finite amplitude by day 20, and over a period of a further week or so lead to the breakup of the mixed patch. The dense fluid that defined the cylinder at $t = 0$ has, by $t = 50$ days, broken up and been dispersed by geostrophic eddies over the whole of the (doubly periodic) domain at its neutrally buoyant level.[1]

This, then, is the mechanism on which we focus here. Before going on to analyze this and further experiments in more detail, we develop some theoretical insight and predictions that will guide in the planning and analysis of those experiments.

2. Theory

If b is the buoyancy defined by

$$b = -g\frac{\sigma}{\rho_0}, \tag{2.1}$$

where g is the acceleration due to gravity, σ the potential density, and ρ_0 a constant reference value of density of water, then the buoyancy difference between the dense mixed column and the lighter ambient fluid (with constant N^2) at any depth will be (see Fig. 2)

$$\Delta b = \Delta b_s\left(1 + \frac{z}{h}\right), \tag{2.2a}$$

where

$$\Delta b_s = N^2 h \tag{2.2b}$$

is the buoyancy difference at the surface and $\Delta b = 0$ at $z = -h$.

If the change in b occurs over a lateral distance μ, then we may deduce the strength of the vertical shear from the thermal wind equation:

$$\frac{\partial u}{\partial z} = \frac{1}{f}\frac{\Delta b}{\mu} \tag{2.3}$$

and it is of cyclonic sense if the cylinder is denser than its surroundings.

Combining (2.1) and (2.3), integrating vertically from ($z = -h$) to ($z = 0$), we obtain

$$u = \frac{h^2N^2}{f\mu}\left(\frac{1}{2}\frac{z^2}{h^2} + \frac{z}{h} + \frac{1}{3}\right), \tag{2.4}$$

where we have chosen the integration constant to ensure that the vertical integral of u vanishes over the range $-h \to 0$.

Now, if the cylinder of dense fluid has a radius that is greater than the ambient radius of deformation based on the depth of the column

[1] Observations show that the ambient stratification is surface intensified, with very weak stratification in the body of the fluid (presumably the consequence of mixing by previous convection). Thus, to compare more directly with observations the experiment shown here, in which N^2 is a constant, must be modified. In section 4 we present a calculation in which N^2 has a more realistic vertical variation.

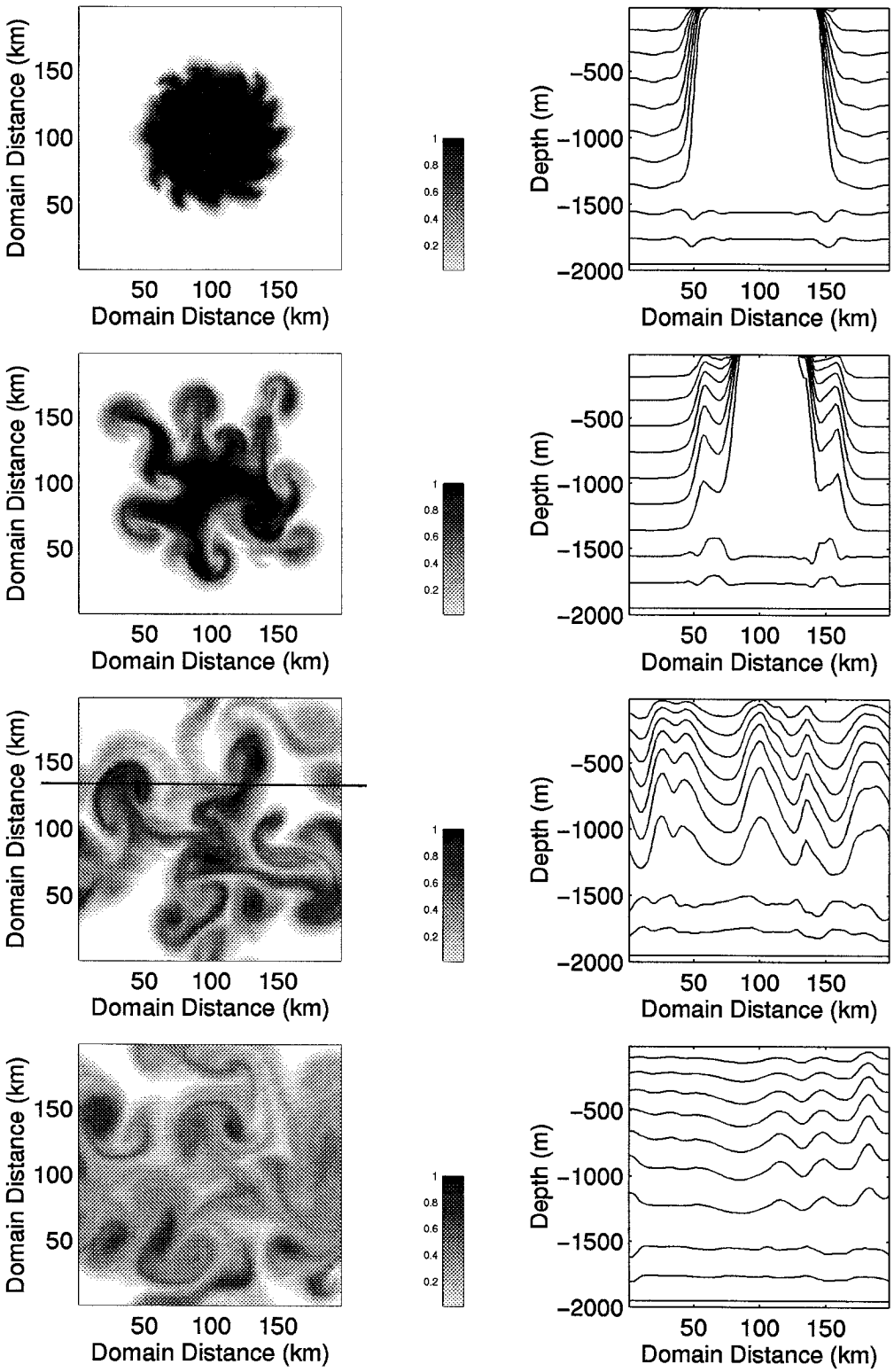

FIG. 3. Numerical illustration of the baroclinic instability of a cylinder of dense fluid, of depth 1500 m and radius 50 km in an ambient fluid in which $N/f = 5$. This is run 4 of Table 1. The plan view panels on the left chart the development of a passive tracer toward the base of the cylinder at a depth of 1400 m after 5, 10, 35, and 50 days. On the right we show a hydrographic section of density through the center of the cylinder at the same times. By day 50 the convected fluid has been spread by eddies over the entire (doubly periodic) domain. The black line in the third panel down on the left indicates the position of the tracer section shown in Fig. 9.

$$L_\rho = \frac{Nh}{f}, \tag{2.5}$$

then baroclinic instability analysis (reviewed in the appendix), laboratory experiment (Saunders 1973), and numerical calculation (for example, see Jones and Marshall 1993 or Herman and Owens 1993) all indicate that the column will become baroclinically unstable. Baroclinic waves will grow, reach finite amplitude, and begin the process of breaking the column up, restratifying the interior, and carrying the broken fragments of the patch away.

The subsequent evolution of the integral properties of the column of ocean will then depend on the interplay between surface buoyancy loss (if it persists) and lateral buoyancy flux by baroclinic eddies, thus

$$\frac{\partial}{\partial t}\int_{\substack{\text{volume of}\\ \text{cylinder}}} \overline{b}\, dV + \oint_{\substack{\text{sides of}\\ \text{cylinder}}} \int_{-h}^{0} \overline{v'b'}\cdot\mathbf{n}\, dl = \int_{\substack{\text{surface of}\\ \text{cylinder}}} \mathcal{B}\, ds, \tag{2.6}$$

where $\overline{v'b'}\cdot\mathbf{n}$ is the lateral eddy buoyancy flux through the sides of the cylinder (with normal unit vector $\mathbf{n}$), $\mathcal{B}$ is the buoyancy flux through the sea surface, and any fluxes associated with entrainment at its base have been neglected.

Equation (2.6) is obtained by integrating the buoyancy equation over the Eulerian volume defined by the initial position of the cylinder of convected fluid. The overbar represents a time average over a suitable averaging period and the ''prime'' the ''eddy component,'' the departure from that mean. Note that we have specifically excluded contributions from ageostrophic advection (as in surface Ekman layers, for example—we mention their possible role later). Furthermore, by the symmetry of the idealized problem that has been set up, advection by the mean geostrophic flow plays no role in the buoyancy budget of the mixed patch.

We now close for the eddy buoyancy flux by assuming

$$\overline{v'b'} = c_e \Delta b u|_{z=0}, \tag{2.7}$$

where c_e is a constant that characterizes the efficiency of eddy transfer across the front.

Substituting for Δb and $u|_{z=0}$ from (2.1) and (2.4), we obtain upon integration

$$\int_{-h}^{0} \overline{v'b'}\cdot\mathbf{n}\, dz = \frac{c_e}{6}\frac{N^4h^4}{\mu f}. \tag{2.8}$$

Having adopted a closure (2.7) for the eddy flux leading to (2.8), we now inquire in to its consequences by solving Eq. (2.6) in two limiting cases.

(i) *Steady state*. The tendency term in (2.6) is assumed to be zero; we suppose that buoyancy loss at the surface persists and solve for the *equilibrium depth* of the statistically steady state in which baroclinic eddies draw buoyancy in from the sides to offset loss from the surface. This has been the subject of recent studies by, for example, Legg and Marshall (1993), Brickman (1995), and Visbeck et al. (1996).

Combining (2.6) and (2.8), setting the tendency term to zero, and $\mu = L_\rho$, we solve for the equilibrium depth to obtain

$$h = \gamma\frac{(\mathcal{B}r)^{1/3}}{N}, \tag{2.9a}$$

where

$$\gamma = \left(\frac{3}{c_e}\right)^{1/3}. \tag{2.9b}$$

The result (2.9a) is the key finding of Visbeck et al. (1996), although the derivation here is somewhat simpler.

Extensive numerical and laboratory studies (Visbeck et al. 1996; Whitehead et. al. 1996) support the parametric dependence of h on $\mathcal{B}$, r, and f suggested by (2.9a) and allow us to determine that the constant of proportionality in Eq. (2.9a) (which is found to be $\approx$4), an important point to which we return in section 3 below.

(ii) *Restratification.* The right hand side of (2.6) is now set to zero; we suppose that buoyancy loss from the surface has ceased and the eddies flux buoyancy in laterally from the ambient fluid, restratifying the homogenized patch. We can estimate a *restratification timescale,* thus,

$$\frac{\partial}{\partial t}\int_{\text{cylinder}} \overline{b}\, dV = -2\pi r \int_{-h}^{0} \overline{v'b'}\cdot\mathbf{n}\, dz,$$

or, dividing both sides by ($\pi r^2 h$), the initial volume of the cylinder, and using (2.8) we find

$$\frac{\partial \hat{b}}{\partial t} = \frac{c_e}{3}\frac{N^3h^2}{r}, \tag{2.10a}$$

where

$$\hat{b} = \frac{1}{\pi r^2 h}\int_{\text{cylinder}} \overline{b}\, dV \tag{2.10b}$$

is the mean buoyancy/unit volume over the cylinder of ocean defined by the initial position of the cylinder defining the convected fluid.

The timescale required to return the buoyancy anomaly within the cylinder to zero can be computed as follows: Using (2.1) and (2.2) we express

$$\frac{\partial \hat{b}}{\partial t} = \frac{1}{\tau_{\text{restrat}}}\left(\frac{1}{2}N^2h - 0\right)$$

and equating to (2.10a) we find that the restratification timescale is given by

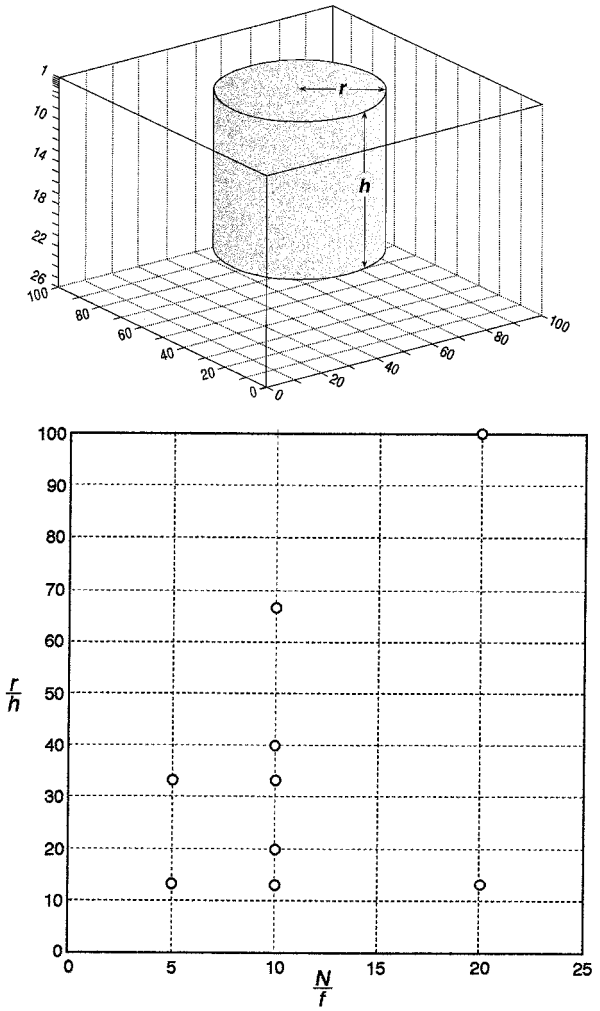

FIG. 4. Numerical setup showing the initial position of the cylinder of dense fluid (a) and the range of r/H and f/N covered by our experiments (b).

$$\tau_{\text{restrat}} = \frac{3}{2c_e}\frac{r}{Nh}. \tag{2.11}$$

It depends on the radius of the mixed patch divided by the velocity scale Nh. In the next section numerical experiments will be used to test the relations in (2.10a) and (2.11) and to determine the constant c_e.

3. Numerical experiments

a. Setup

The incompressible Navier–Stokes model described in Marshall et al. (1997a,b) was configured in a doubly periodic domain of side L and depth H. The horizontal resolution of the model was 2 km in all calculations; the vertical resolution decreased from ~20 m at the surface to 100 m in the interior. The domain was filled with a linearly stratified fluid (N^2 = const) except over a cylinder centered in the middle of the domain. A linear equation of state of the form $\rho = \rho_0(1 - \alpha T')$ was assumed. The patch was prescribed as a column of mixed water within an initially resting, linearly stratified ocean such that $b_{\text{chimney}} = N^2h$; see Fig. 4a. Circular mixed patches of varying depth h and radius r under varying conditions of ambient stratification N and rotation rate f were studied. To suppress artificial asymmetries arising from our attempt to represent a circular plan-form on the square grid, a random ($\pm$) perturbation of order 2 km, the grid scale of the model, was added to the radius.

TABLE 1. Experimental parameters for the 13 runs.

Run	r (km)	h (m)	N (s^{-1})	f (s^{-1})	Stable
1	20	1500	2×10^{-3}	10^{-4}	Yes
2	20	1500	10^{-3}	10^{-4}	
3	20	1500	0.5×10^{-3}	10^{-4}	
4	50	1500	0.5×10^{-3}	10^{-4}	
5	20	500	10^{-3}	10^{-4}	
6	100	1500	10^{-3}	10^{-4}	
7	50	1500	10^{-3}	10^{-4}	
8	20	1500	10^{-3}	2×10^{-4}	
9	20	1500	10^{-3}	0.5×10^{-4}	Yes
10	20	1000	10^{-3}	10^{-4}	
11	50	500	2×10^{-3}	10^{-4}	
12	100	1000	2×10^{-3}	10^{-4}	
13	50	1500	10^{-3}	2×10^{-4}	

The fluid contained in the cylinder was tagged with a passive tracer that was allowed to evolve, aiding in the identification of the pathways of water that, at $t = 0$, made up the cylinder. There was no externally implied mechanical or thermodynamic forcing.

Laplacian diffusion of density, momentum, and tracer was employed with constant coefficients reduced to the minimum required to maintain numerical coherency on the grid scale of the model. Many experiments were carried out to satisfy ourselves that the gross properties of the mixed patch and its fragmentation through baroclinic instability were insensitive to the choices made (provided, of course, that the diffusion terms were large enough to ensure numerical stability). A value of $K_h = 10\ m^2\ s^{-1}$ was found to be satisfactory, implying a diffusive timescale of several years over 50 km, a typical cylinder radius, much longer than typical restratification timescales of 50 days or so.

There are two key nondimensional numbers that characterize our system, one which is purely geometrical r/H, and the other which depends on internal properties f/N. The ratio of the two is just r/L_ρ. Thirteen or so experiments were carried out; they are set out in Table 1 and the range of r/H and f/N covered by them plotted in Fig. 4b. The procedure was the same in each case. The cylinder was allowed to evolve freely until it had been completely broken into fragments and dispersed by eddies. The mean buoyancy $\bar{b}$ contained within an Eulerian cylinder, defined by the initial position of the dense water, was diagnosed periodically during the integration and currents and tracer sections plotted.

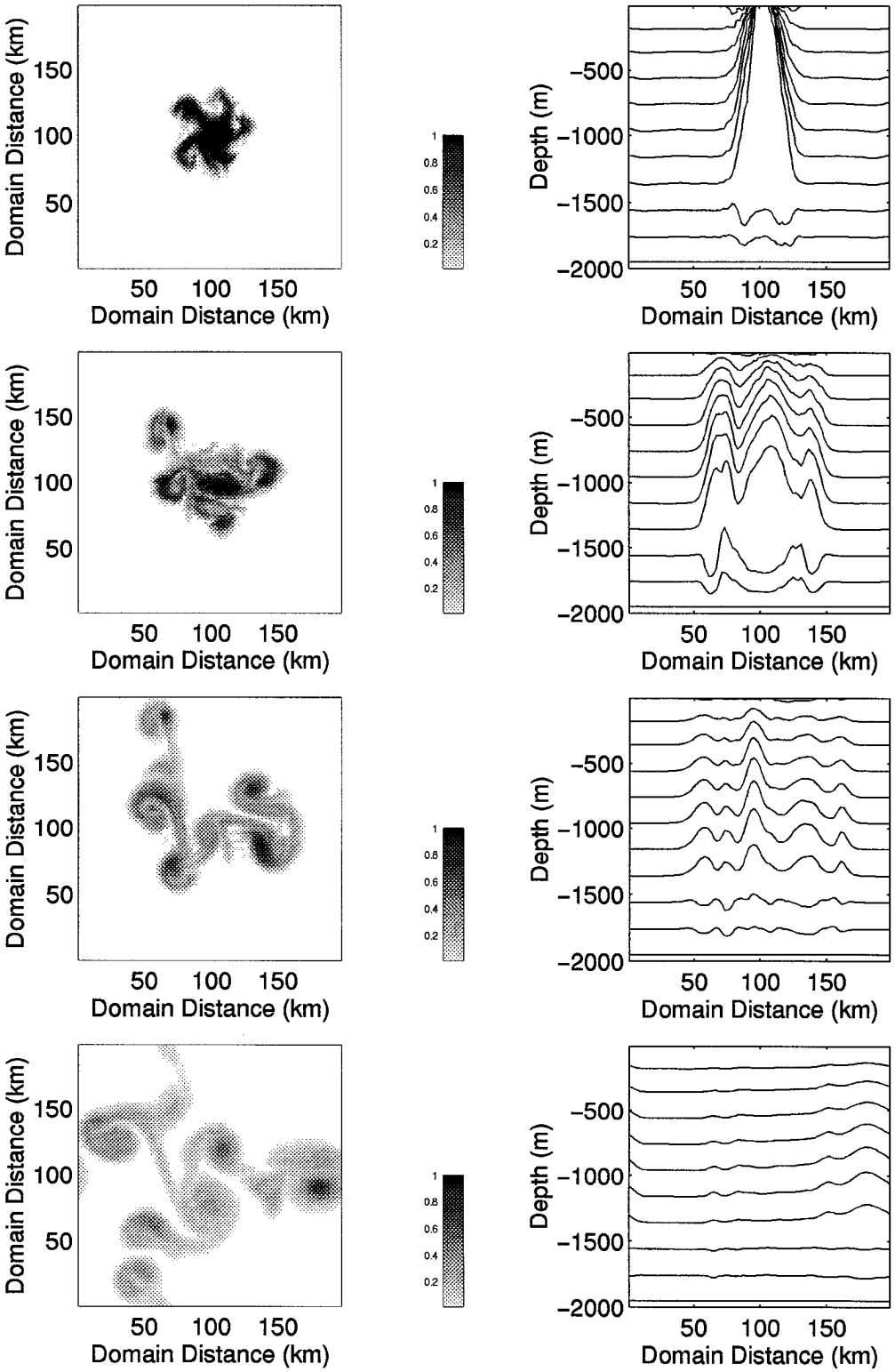

FIG. 5. A mode-5 breakup of a cylinder of radius 20 km and depth 1500 m in an ambient fluid in which $N/f = 10$. The plots are shown at days 3, 7, 12, and 20. This is run 2 of table 1. The format is as in Fig. 3.

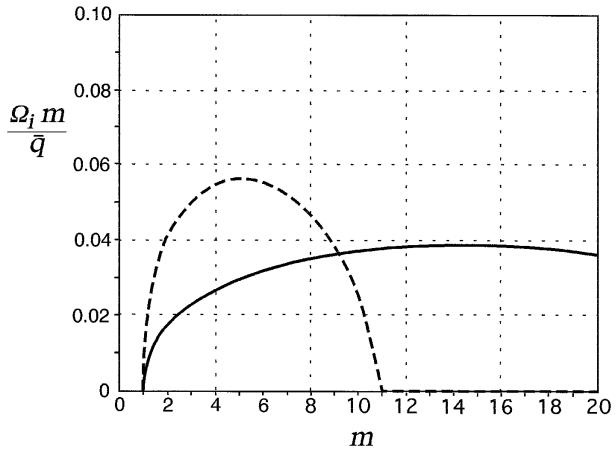

FIG. 6. The linear growth rate of eddies on the rim current surrounding the mixed patch as a function of mode number, deduced from two-layer quasigeostrophic theory (outlined in the appendix). The dotted line is for the experiment shown in Fig. 5 (run 2) and the continuous line for the experiment shown in Fig. 3 (run 4). The curves were plotted using Eq. (A.4).

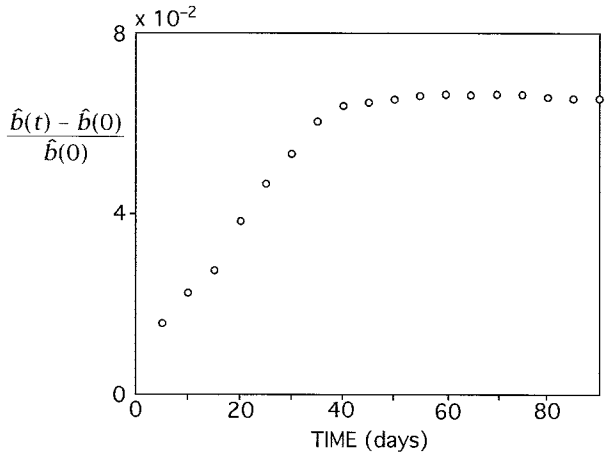

FIG. 7. Plot of $\hat{b}$ [Eq. (2.10b)] as a function of time diagnosed from run 4 (Fig. 3).

b. Results

Figure 3, described in the introduction, charts the evolution of the cylinder in run 4 (Table 1). There the cylinder had a radius very much larger than the deformation radius, leading to a mode-14 instability. Figure 5, from run 8 with a much smaller radius, shows a mode-5 breakup. To the extent that we can assume that the initial configuration is amenable to a quasigeostrophic analysis (see the appendix for details) linear theory is a useful guide to the growth rate and scale of the fastest-growing mode. The results of such an analysis are presented in Fig. 6 for the experiments shown in Figs. 3 and 5; the analysis is able to predict the initial scale of the growing waves and their growth rate. In each case, however, and perhaps not surprisingly, we find that linear theory is only a useful predictor of the initial phase of the instability; we observe that the eddies merge and grow in scale as their amplitude increases.

A matrix of disintegrating cylinder experiments was carried out with the parameters given in Table 1. In each case the mode number of the instability can be anticipated from linear theory, and as eddies grow to finite amplitude they restratify the column and carry the mixed fluid away. As we now go on to demonstrate, the dependence of the restratification timescale on external parameters is well predicted and can be understood in terms of Eq. (2.11). Moreover, the experiments can also be used to define the constant c_e.

Figure 7 plots $\hat{b}$ as a function of time diagnosed from run 4 (Fig. 3). We see that $\hat{b}$ increases in a roughly

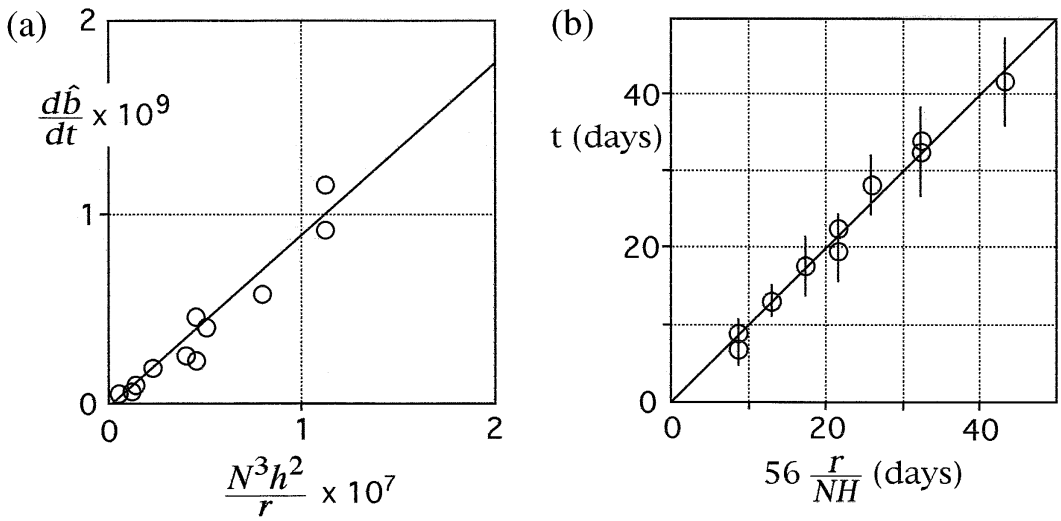

FIG. 8. (a) The observed $d\hat{b}/dt$ plotted against the theoretical prediction N^3h^2/r, Eq. (2.10), for each of the runs in Table 1. (b) The observed $\tau_{restrat}$ plotted against $56(r/Nh)$ for each run.

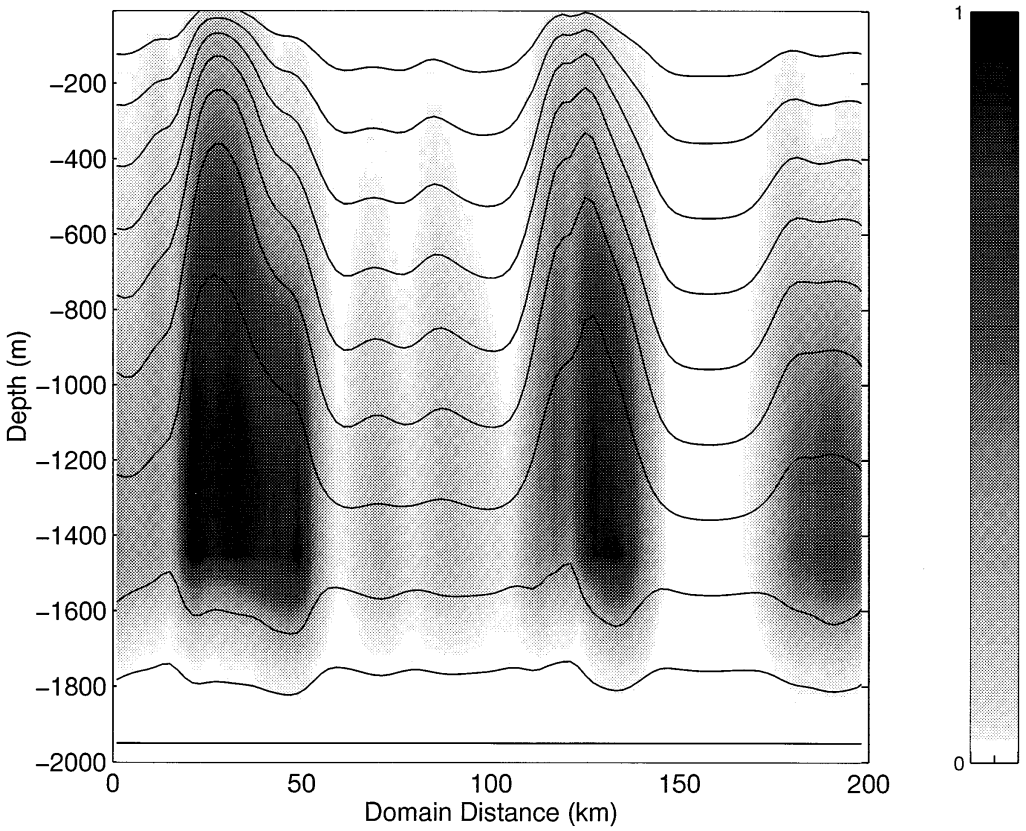

FIG. 9. Vertical cross section of tracer (grayscale) and temperature (contoured) through the breaking mixed patch plotted in run 4 showing convected water spreading far from the formation region. The black line in Fig. 3 indicates the position of the section.

linear manner with time until, after 40 days or so, it reaches a steady value corresponding to the eradication of the buoyancy anomaly of the initial state. For each of the experiments tabulated in Table 1, we estimate $d\hat{b}/dt$ from the slope of the rising curve (such as in Fig. 7) and τ_{restrat} from the time it takes to restore the buoyancy deficit over the cylinder to that of the ambient fluid.

The observed $d\hat{b}/dt$ is plotted in Fig. 8a against our theoretical prediction N^3h^2/r, Eq. (2.10), for each of our runs. Pleasingly the points fall on a roughly straight line. According to our theory the slope of the line is $c_e/3$ [see Eq. (2.10a)], where c_e is the constant in Eq. (2.7); the slope of the line through the points is 0.9×10^{-2} suggesting that $c_e = 0.027$. Indeed taking $c_e = 0.027$, then the constant of proportionality between τ_{restrat} and r/Nh in Eq.(2.11) is

$$\frac{3}{2 \times 0.027} = 56.$$

Thus, in Fig. 8b we plot the observed τ_{restrat} against the prediction $56(r/Nh)$; the agreement must be considered as encouraging and strongly supportive of the theoretical ideas set out in section 2. We now go on to consider whether such a value of c_e is reasonable in the light of previous studies.

In the studies of Visbeck et al. (1996) and Whitehead et al. (1996), numerical and laboratory experiments were performed and analyzed in which buoyancy was constantly extracted over a circular patch at the surface. Instead of deepening indefinitely, the baroclinic eddies induced by the cooling arrested the deepening and led to a statistically steady state characterized by a depth h_{equil}. The theory of section 2a predicts that the equilibrium depth is given by Eq. (2.9). If $c_e = 0.027$, then the constant of proportionality between the equilibrium depth and $(\mathcal{B}r)^{1/3}/N$ is $(3/c_e)^{1/3} = (3/0.027)^{1/3} = 4.8$. This should be contrasted with the value obtained by Visbeck et al. (1996) of 3.9 ± 0.9 and by Whitehead et al. (1996) of 4.6 ± 0.8 in the laboratory. To within error bars the three estimates are the same.

4. Conclusions

a. *Restratification and dispersal by geostrophic eddies*

Observations show that convectively tainted water can be found many tens, even hundreds, of kilometers away from the site of convection, only a matter of weeks after the meteorology suggests that convection has ceased. Our experiments vividly demonstrate that

TABLE 2. Timescale restrat values for a range of r, N, and h.

	N/f			
r/h	1	5	10	50
1	56	11	6	1
10	560	112	56	11
50	2800	560	280	56
100	5600	1120	560	112

geostrophic eddies, spawned by the baroclinic instability of the mixed patch, can indeed rapidly disperse the convectively mixed water, carrying it speedily from its formation region. For example, Fig. 9 shows a vertical (hydrographic) section along the line marked in Fig. 3. We observe ''blobs'' of mixed fluid being carried away from the convective site. As the convected water is advected away, eddies draw stratified water inward at the surface. One is reminded of the meteorological analog in which synoptic eddies sweep warm fluid poleward on rising trajectories and cold air equatorward on sinking trajectories; the center of the patch assumes the role of the atmospheric pole.

Our experiments support the theoretical predictions made in section 2 and provide a calibration to tie down the parameter c_e; a $c_e = 0.027$ is implied. The implications are best summarized in Table 2 where the timescale $\tau_{\text{restrat}} = 56(r/Nh)$ is tabulated for a range of values of r, N, and h. For example, suppose that we assume $r = 140$ km, $N = 10^{-3}$ s^{-1}, $f = 10^{-4}$ s^{-1}, and $h = 1400$ m, not untypical of the MEDOC mixed patch observed by Schott and Send in the Western Mediterranean in 1994. Then $N/f = 10$; $r/h = 100$, and the eddy transfer mechanism implies a restratification timescale $\tau f \sim 560$ or $\tau_{\text{restrat}} = 56$ days, more or less as is observed.

Before concluding we draw attention to one perhaps unrealistic aspect of the experiments presented thus far; N^2 is assumed to be constant with depth in the ambient field. However, observations show that the ambient stratification of convection sites is typically strongly surface intensified—the stratification at middepths is often very weak, a consequence of recurring vertical mixing during convection. In Fig. 10, therefore, we present sections through a disintegrating patch in which the stratification is indeed surface intensified (see legend for details). The same basic mechanism operates as before; baroclinic instability sets in but now the restratification appears as an upper-ocean process on a vertical scale that matches that of the ambient fluid. Figure 10 has a character that more clearly resembles the observations—see, for example, the AR7 section across the Labrador Sea taken by Lazier (1994, personal communication). It clearly shows that by the summer following wintertime convection the fluid column has been restratified to a depth of about 500 m across the whole extent of the

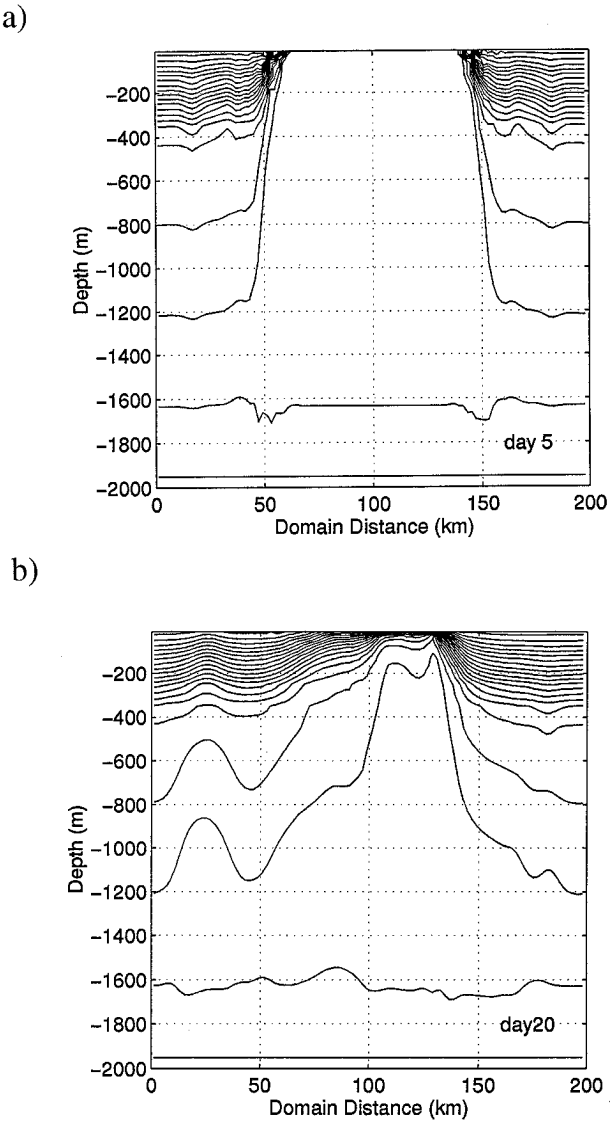

FIG. 10. Hydrographic section through a mixed patch breaking up into an ambient fluid in which the stratification is surface intensified. In the top 500 m $N = 2 \times 10^{-3}$ s^{-1}; beneath $N = 0.5 \times 10^{-3}$ s^{-1}. Otherwise all parameters are as in run 4 (Fig. 3).

section running from Labrador to Greenland. The conclusion of the present study is that a likely restratification mechanism is lateral eddy transport of fluid from the buoyant boundary current that surrounds the convection site. How might we apply our formula in this context? If the stratified layer has a depth h and is characterized by a density jump across it of magnitude Δb, then it is useful to write (2.11) in the form

$$\tau_{\text{restrat}} \approx 56 \frac{r}{(h\Delta b)^{1/2}}.$$

Choosing $h = 500$ m, $\Delta b = 2 \times 10^{-3}$ m s^{-2}, $r = 200$ km, broadly consistent with Labrador Sea conditions,

we find that $\tau_{\text{restrat}} \equiv 100$ days, a plausible timescale and not inconsistent with the fragmentary observational evidence that is currently available in the Labrador Sea.

Finally, we mention other possible mechanisms of restratification and dispersal that might play an important role here and elsewhere. A mixed body of fluid that abuts a boundary will excite boundary waves (Kelvin and topographic Rossby waves), which are forerunners of the ''bleeding'' of the convected fluid away from the reservoir in boundary currents. This has been studied in numerical simulations (Madec and Crepon 1991), laboratory experiments, and is hinted at in the observations presented by Send et al. (1995). Wind-driven Ekman-layer processes are likely to play a role in the advective supply of stratified fluid to the convection site. However, it is not yet clear whether ageostrophic advection is of the appropriate sign or magnitude to account for the very efficient restratification process observed to occur over a rather deep surface layer.

The unraveling of the relative importance of these competing processes during each stage of the convective process demands further observations in the light of theoretical and numerical study.

Acknowledgments. Helen Jones received support from EEC through MAST. John Marshall was supported through an NSF grant and the Office of Naval Research. Most of the thinking and some of the details of the present study were worked out when the authors were taking part in the 1995 GFD Summer School on ''Rotating Convection'' in Woods Hole. The numerical simulations were carried out on the CM5 housed in the Laboratory for Computer Science at MIT supported by the SCOUT project.

APPENDIX

Linear Stability Analysis of a Two-Layer Baroclinic Vortex

By viewing the mixed patch from a potential vorticity perspective we are able to couch a stability problem that successfully predicts the growth rate and scale of the eddies that grow on the thermal wind around the periphery of the patch.

Legg and Marshall (1993) describe how a homogeneous patch of fluid can be modeled as a two-layer vortex of the kind sketched in Fig. A1. The cold surface (following Bretherton 1966) is represented as a thin sheet of *positive* (quasigeostrophic) potential vorticity q_s, and the mixed core by an extended *negative* value of potential vorticity q_i, and the q are chosen to satisfy the condition

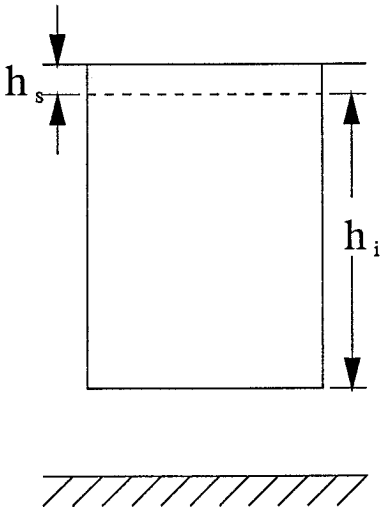

FIG. A1. Schematic of the chimney as a two-layer baroclinic vortex.

$$\int_{\substack{\text{mixed}\\ \text{patch}}} q \, dV = 0. \tag{A.1}$$

This is ensured by setting $q_s = (\overline{q}/\sqrt{\delta}$ and $q_i = -\sqrt{\delta}\,\overline{q}$, where

$$\delta = \frac{h_s}{h_i} \tag{A.2}$$

and h_s and h_i are the depths of the upper and lower layers respectively such that $h_i + h_s = h$ is the total depth of the mixed patch, and $\overline{q}$ is a measure of the absolute strength of the vortex.

Using the method set out, for example, in Pedlosky (1985), it can be shown that if there is no barotropic component to the flow, the phase speed of infinitesimal wavelike perturbations of azimuthal wavenumber m is given by

$$\Omega = \frac{1}{2}\varepsilon\overline{q}(I_1K_1 - I_mK_m) \pm \frac{1}{2}\overline{q}\sqrt{\frac{I_mK_m}{2m}[2m\varepsilon^2(I_1K_1 - I_mK_m) + 4(2mI_1K_1 - 1)]\left(\frac{I_1K_1}{I_mK_m} - 1\right)}, \tag{A.3}$$

where

$$\varepsilon = \left(\frac{1 - \delta}{\sqrt{\delta}}\right).$$

The mth order Bessel functions I_m, K_m are evaluated at a/λ, where "a" is the radius of the mixed patch and λ is a deformation radius

$$\lambda = \frac{2\sqrt{\delta}}{1 + \delta}\lambda_0,$$

in which $\lambda_0 = Nh/(\sqrt{2}f)$. Thus, we see that by decreasing the ratio of the upper to the lower layer depth, the deformation radius is decreased.

From (A.3) it is readily shown that the sufficient condition for instability (complex Ω) is

$$\left(I_1K_1 - \frac{1}{2m}\right) > \frac{\varepsilon^2}{4}(I_1K_1 - I_mK_m),$$

so that the growth rate of an unstable wave of mode number m, as measured by the imaginary part of (A.3), is

$$\Omega_i m = \frac{1}{2}\bar{q}m\sqrt{I_mK_m\left[\varepsilon^2(I_1K_1 - I_mK_m) + 4\left(\frac{1}{2m} - I_1K_1\right)\right]\left(\frac{I_1K_1}{I_mK_m} - 1\right)}. \quad \text{(A.4)}$$

Assuming $\delta = \Delta z_{\text{top}}/(h - \Delta z_{\text{top}})$, where Δz_{top} is the depth of the upper layer of the numerical model and h is the depth of the patch, we are able to predict the growth rate as a function of m—see Fig. 6 where $\Omega m\bar{q}$ is plotted as a function of m.

REFERENCES

Bretherton, F. P., 1966: Critical layer instability in baroclinic flows. *Quart. J. Roy. Meteor. Soc.*, **92,** 325–334.

Brickman, D., 1995: Heat flux partitioning in open-ocean deep convection. *J. Phys. Oceanogr.*, **25,** 2609–2623.

Hermann, A. J., and W. B. Owens, 1993: Energetics of gravitational adjustment for mesoscale chimneys. *J. Phys. Oceanogr.*, **23,** 346–371.

Jones, H., and J. Marshall, 1993: Convection with rotation in a neutral ocean: A study of open-ocean deep convection. *J. Phys. Oceanogr.*, **23,** 1009–1039.

Legg, S., and J. Marshall, 1993: A heton model of the spreading phase of open-ocean deep convection. *J. Phys. Oceanogr.*, **23,** 1040–1056.

Madec, G., and M. Crepon, 1991: Thermohaline driven deep-water formation in the Northwestern Mediterranean Sea. *Deep Convection and Deep Water Formation in the Oceans,* P. C. Chu and J. C. Gascard, Eds., Elsevier Science, 241–265.

Marshall, J., C. Hill, L. Perelman, and A. Adcroft; 1997a: Hydrostatic, quasi-hydrostatic and non-hydrostatic ocean modelling. *J. Geophys. Res.*, **102** (C3), 5733–5752.

——, A. Adcroft, C. Hill, L. Perelman, and C. Heisey, 1997b: A finite-volume, incompressible Navier–Stokes model for studies of the ocean on parallel computers. *J. Geophys. Res.*, **102** (C3), 5753–5766.

MEDOC Group, 1970: Observations of formation of deep water in the Mediterranean Sea, 1969. *Nature*, **227,** 1037–1040.

Pedlosky, J., 1985: The instability of continuous heron clouds. *J. Atmos. Sci.*, **42,** 1477–1486.

Saunders, P. M., 1973: The instability of a baroclinic vortex. *J. Phys. Oceanogr.*, **3,** 61–65.

Send, U., F. Schott, F. Gaillard, and Y. Desaubies, 1995: Observation of a deep convection regime with acoustic tomography. *J. Geophys. Res.*, **100** (C4), 6927–6941.

THETIS Group (F. Schott, U. Send, G. Krahmann, C. Mertens, M. Rhein, M. Visbeck, Y. Desaubies, F. Gaillard, T. Terre, M. Taroudakis, G. Athanassoulis, and E. Skarsoulis), 1994: Open-ocean deep convection explored in the Mediterranean. *Eos, Trans. Amer. Geophys. Union*, **75** (19), 217–221.

Visbeck, M., J. Marshall, and H. Jones, 1996: Dynamics of isolated convective regions in the ocean. *J. Phys. Oceanogr.*, **26,** 1721–1734.

Whitehead, J., J. Marshall, and G. Hufford, 1996: Localized convection in rotating stratified fluid. *J. Geophys. Res.*, **101** (C10), 25 705–25 721.

Worcester, P. F., J. F. Lynch, W. M. L. Morawitz, R. Pawlowicz, P. J. Sutton, B. D. Cornuelle, O. M. Johannessen, W. H. Munk, W. B. Owens, R. Shuchman, and R. C. Spindel, 1993: Evolution of the large-scale temperature field in the Greenland Sea during 1988–89 from tomographic measurements. *Geophys. Res. Lett.*, **20** (20), 2211–2214.